Synthetic Methods for Perovskite Materials – Structure and Morphology

Ana Ecija, Karmele Vidal, Aitor Larrañaga,
Luis Ortega-San-Martín and María Isabel Arriortua
[1]*Universidad del País Vasco/Euskal Herriko Unibertsitatea (UPV/EHU), Facultad de Ciencia y Tecnología, Dpto. Mineralogía y Petrología, Leioa,*
[2]*Pontificia Universidad Católica del Perú (PUCP), Dpto. Ciencias, Sección Químicas, Lima,*
[1]*Spain*
[2]*Perú*

1. Introduction

Solid state chemistry thrives on a rich variety of solids that can be synthesized using a wide range of techniques. It is well known that the preparative route plays a critical role on the physical and chemical properties of the reaction products, controlling the structure, morphology, grain size and surface area of the obtained materials (Cheetham & Day, 1987; Rao & Gopalakrishnan, 1997). This is particularly important in the area of ABO_3 perovskite compounds given that they have for long been at the heart of important applications. From the first uses of perovskites as a white pigments, $PbTiO_3$ in the 1930's (Robertson, 1936) to the MLC capacitors (mostly based in substituted $PbTi_{1-x}Zr_xO_3$ or $BaTiO_3$ materials) in which today's computers rely on to operate, synthetic methods have been a key factor in the optimization of their final properties (Pithan et al., 2005).

Traditionally, most of these ceramic materials have been prepared from the mixture of their constituent oxides in the so called solid state reaction, "shake and bake" or ceramic method, a preparative route for which high temperature is a must in order to accelerate the slow solid–solid diffusion (Fukuoka et al., 1997; Inaguma et al., 1993; Safari et al., 1996). Despite its extended use in practically all fields in which perovskite-structured materials are needed, not all applications are better off with this method since the low kinetics and high temperature also yield samples with low homogeneity, with the presence of secondary phases and with uncontrolled (and typically large) particle size of low surface area which are undesired for some applications such as in gas sensors or in catalysis where small particles and high surface area are needed (Bell et al., 2000). This conventional route, however, is widely employed due to its simplicity and low manufacturing cost. Nevertheless, with appropriate optimisation, as when soft-mechanochemical processing is used prior to calcinations at high temperature (Senna, 2005), the method results in high quality single phase perovskites that can be used in electroceramic applications.

Alternative routes to the solid-state reaction method are wet chemical synthetic methods such as co-precipitation (with oxalates, carbonates, cyanides or any other salt precursors), combustion (including all variants from low to high temperature), sol–gel (and all of its modifications with different chelating ligands), spray-pyrolysis, metathesis reactions, etcetera (Patil et al., 2002; Qi et al., 2003; Royer et al., 2005; Segal, 1989; Sfeir et al., 2005). In all cases the idea is to accelerate the pure phase formation, a goal that is achieved due to the liquid media which permits the mixing of the elements at the atomic level resulting in lower firing temperatures. Other advantages of these methods are the possibility of having controlled particle size, morphology and improvement in surface area.

In most cases, the final microstructure of the sample is the key issue in choosing the synthetic method, but phase purity is also a must, and is sometimes overlooked when authors praise their particular synthetic method (Kakihana & Yoshimura, 1999). This was pointed out by Polini et al. (Polini et al., 2004) in the case of the preparation of substituted $LaGaO_3$ phases for SOFC cathodes: methods that supposedly have been developed to improve the scalability and uniformity of the samples, such as the Pechini method (a particular case of the sol-gel method), do not always result in a single phase of the crystalline sample required. Similar cases are common in the literature, as in the case of $La_{1-x}Sr_xMnO_{3-\delta}$ phases (Conceição et al., 2009). This clearly indicates that there is not such a thing as the ideal synthetic method: every method has its advantages and disadvantages.

Ideally, as many as possible synthetic methods should be tried and optimised for each compound of interest in order to obtain better crystals with the proper microstructure. But this is obviously time consuming and very costly. Consequently, researchers usually choose to follow the general trends that have been observed to work in a particular area of interest. As a result, each field has its preferences. For example, the ceramic method, widely used at the beginning of the first years of the high-Tc superconductors was soon replaced because it almost always resulted in non-stoichiometric products with some undesired phases that complicated the interpretation of the superconducting properties. These materials got so much attention in the late 1980's and early 1990's that completely new synthesis methods were introduced including many modifications of sol-gel methods with the ample use of alcoxides as precursors (Petrikin and Kakyhana, 2001). In this case, the synthetic route consisted on the preparation of mixed coordination compounds with alcoxy ligands in aqueous media which ensured good distribution of all metals involved and yielded purer superconducting oxides at relatively lower temperatures than before.

On the other hand, combustion methods (glycine-nitrate, urea based, and other modifications) have been proposed as one of the most promising methods to prepare perovskite oxide powders to be used as cathode materials in Solid Oxide Fuel Cell technology. (Bansal & Zhong, 2006; Berger et al., 2007; Dutta et al., 2009; Liu & Zhang, 2008). This method consist on a highly exothermal self-combustion reaction between the fuel (usually glycine, urea or alanine) and the oxidant (metal nitrates), that produces enough heat to obtain the ceramic powders. Compared to the ceramic method this synthetic route has much faster reaction times and lower calcination temperatures leading to powders with large compositional homogeneity and nanometric particle sizes, which are desired characteristics for this type of application.

For some applications, such as in multiferroic materials based devices, it is the crystal symmetry of the multiferroic what matters. In these materials the presence or not of a centre of symmetry is crucial for the observation of ferroelectricity. With this regard, there are cases, as in some $AMnO_3$ perovskites (A=Y or Dy), in which the synthetic route determines whether an orthorhombic compound with a centre of symmetry (i.e. non ferroelectric) or a hexagonal phase without the centre (i.e. ferroelectric) is formed (Carp et al., 2003; Dho et al., 2004). Consequently, preparative conditions have to be carefully selected in order to obtain crystal phases with the adequate structure. The use of more than one synthesis method is thus worth trying in all cases.

In this work three different groups of perovskite compounds have been prepared and their crystal structure and microstructure have been studied using X-ray diffraction (XRD) and scanning electron microscopy (SEM). Each group of samples had its own structural characteristics so, prior to choosing one synthetic approach, trials were carried out using different methods. In all cases, the final method chosen was the one that maximised phase purity and resulted in better properties. Here we demonstrate that phase pure samples susceptible to be compared depending on the desired characteristics can be obtained using different synthetic methods.

2. Experimental

Up to four different synthetic methods (solid state reaction, glycine-nitrate route, sol-gel and freeze-drying) have been used to synthesize a group of 14 perovskite compounds (Figure 1), which have the potential for their use in different applications.

Compound	Synthetic method	Variable		Label
$La_{0.50}Pr_{0.30}Sr_{0.20}FeO_{3-\delta}$	Solid state reaction	x in A	0.2	LPS20
$La_{0.40}Nd_{0.30}Sr_{0.23}Ca_{0.07}FeO_{3-\delta}$	Solid state reaction		0.3	LNSC30
$La_{0.20}Pr_{0.40}Sr_{0.26}Ca_{0.14}FeO_{3-\delta}$	Solid state reaction		0.4	LPSC40
$La_{0.19}Pr_{0.31}Sr_{0.26}Ca_{0.24}FeO_{3-\delta}$	Solid state reaction		0.5	LPSC50
$La_{0.19}Pr_{0.21}Sr_{0.26}Ca_{0.34}FeO_{3-\delta}$	Solid state reaction		0.6	LPSC60
$La_{0.18}Pr_{0.12}Sr_{0.26}Ca_{0.44}FeO_{3-\delta}$	Solid state reaction		0.7	LPSC70
$La_{0.20}Sr_{0.25}Ca_{0.55}FeO_{3-\delta}$	Solid state reaction		0.8	LSC80
$La_{0.50}Ba_{0.50}FeO_{3-\delta}$	Glycine-nitrate route	$<r_A>$(Å)	1.34	LB134
$La_{0.34}Nd_{0.16}Sr_{0.12}Ba_{0.38}FeO_{3-\delta}$	Glycine-nitrate route		1.31	LNSB131
$La_{0.04}Nd_{0.46}Sr_{0.24}Ba_{0.26}FeO_{3-\delta}$	Glycine-nitrate route		1.28	LNSB128
$La_{0.05}Sm_{0.45}Sr_{0.32}Ba_{0.18}FeO_{3-\delta}$	Solid state reaction		1.25	LSSB125-ss
	Glycine-nitrate route		1.25	LSSB125-gn
$Nd_{0.8}\ Sr_{0.2}\ Mn_{0.9}Co_{0.1}O_3$	Sol-gel	x in B	0.1	NSMC10-sg
	Freeze-drying		0.1	NSMC10-fd
$Nd_{0.8}\ Sr_{0.2}\ Mn_{0.8}Co_{0.2}O_3$	Sol-gel		0.2	NSMC20-sg
	Freeze-drying		0.2	NSMC20-fd
$Nd_{0.8}\ Sr_{0.2}\ Mn_{0.7}Co_{0.3}O_3$	Sol-gel		0.3	NSMC30-sg
	Freeze-drying		0.3	NSMC30-fd

x: doping level in $Ln_{1-x}A_xFeO_{3-\delta}$ and $Nd_{0.8}Sr_{0.2}(Mn_{1-x}Co_x)O_3$ series; $<r_A>$: average ionic radius of A-cation in the $Ln_{0.5}A_{0.5}FeO_3$.

Table 1. Nominal compositions, synthetic methods, and labels of the studied perovskites.

These compounds have been divided into three groups and their compositional details are summarised in Table 1. Preparation procedures are detailed below.

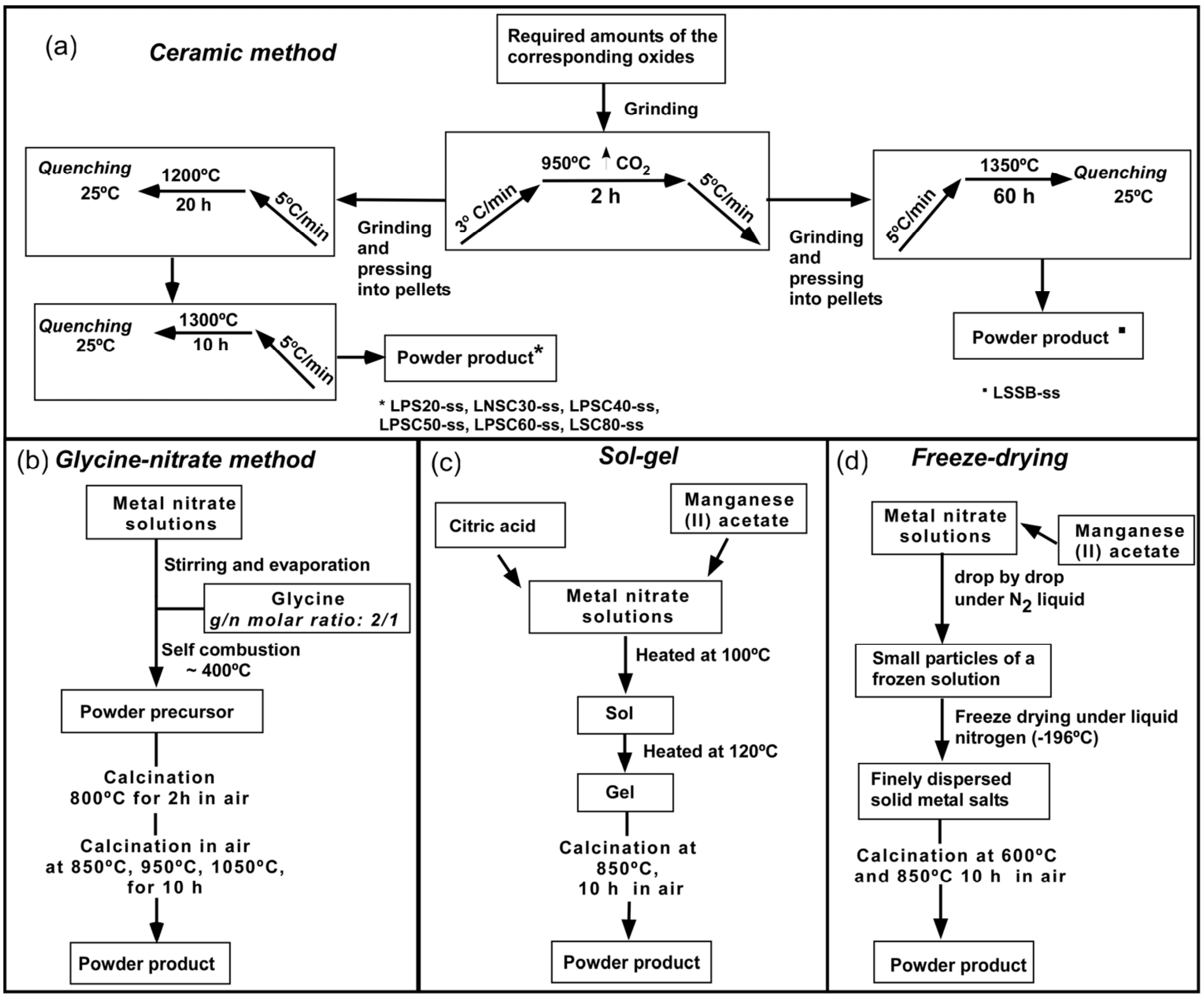

Fig. 1. Flowcharts for the: (a) ceramic, (b) glycine-nitrate, (c) sol-gel and (d) freeze-drying methods used to obtain the perovskite compounds shown in the present work.

The selection of each method and composition for each series of perovskites was based on the desired applications that are described later.

2.1 Ceramic solid state reaction

The compounds prepared via the ceramic route were obtained from mixing stoichiometric amounts of the raw oxides with 2-propanol in an agate mortar. Starting materials were always oxides of high purity such as La_2O_3 (99.99%), Sm_2O_3 (99.999%), Pr_2O_3 (99.9%), Gd_2O_3 (99.99%), BaO (99.99%), SrO (99.9%), CaO (99.9%) and Fe_2O_3 (99.98%). Afterwards, these mixtures were shaped into pellets and were fired in air at 950ºC for 2h. The products obtained were ground, pelletized again and fired at higher temperatures. The flowchart shown in Figure 1a details the heat treatments required in each case until pure samples were obtained.

2.2 Glycine-nitrate route

The preparations of the perovskite compounds with the general composition $Ln_{0.5}A_{0.5}FeO_{3-\delta}$ by glycine-nitrate route involved the use of some nitrates instead of the oxides as starting materials: $Ba(NO_3)_2$ (99.99%), $Sr(NO_3)_2$ (99.9%) and $Fe(NO_3)_3$ (99.98%). The oxides used were La_2O_3 (99.99%), Sm_2O_3 (99.999%), Gd_2O_3 (99.99%). The oxides were dissolved in diluted nitric acid to obtain the corresponding nitrates and the metal nitrates dissolved in distilled water. The solutions were mixed in a 1 litre glass beaker, under constant stirring and placed on a hot plate to evaporate the water excess. After a significant reduction of the solution volume the glycine was added. The amount of glycine used was calculated in order to obtain a glycine/nitrate molar ratio of 2:1. This amino acid acts as complexing agent for metal cations and as the fuel for the combustion reaction. The resulting viscous liquid was auto-ignited by putting the glass beaker directly in a preheated plate (at ~400ºC). The obtained powders were pelletized and fired at 800ºC for 2 hours to remove the carbon residues. The heatings at temperatures above 800ºC were repeated until pure phases were obtained. A flowchart with more details and heat treatments involved in this synthesis is shown in Figure 1b.

2.3 Sol–gel

The sol-gel method was used for the oxides of general composition $Nd_{0.8}Sr_{0.2}(Mn_{1-x}Co_x)O_3$ (x = 0.1, 0.2 and 0.3). Initially, the oxide Nd_2O_3 (99.9%) was dissolved in aqueous nitric acid followed by the addition of $Sr(NO_3)_2$ (99%), $Co(NO_3)_2.6H_2O$ (99%) and $Mn(C_2H_3O_2)_2.4H_2O$ (99%). Citric acid was then used as the quelating agent and ethylene glycol as the sol forming product. The solution was slowly evaporated in a sand bath for 24 h and the gel obtained was subjected to successive heat treatments at the temperature of 850ºC (with intermediate grindings). Each firing was of 10 h and was carried out under nitrogen atmosphere. The flowchart for this synthesis is shown in Figure 1c.

2.4 Freeze-drying technique

In the freeze drying method, standardized nitrate solutions were mixed according to the stoichiometry of the final products: $Nd_{0.8}Sr_{0.2}(Mn_{1-x}Co_x)O_3$ (x = 0.1, 0.2 and 0.3). The starting materials were Nd_2O_3 (99.9%) which had to be dissolved in diluted nitric acid before the addition of the other compound; $Sr(NO_3)_2$ (99%); $Co(NO_3)_2.6H_2O$ (99%) and $Mn(C_2H_3O_2)_2.4H_2O$ (99 %).

The mixture for freeze-drying method was frozen drop-by-drop under liquid nitrogen and subjected to freeze drying at P = 5.10^{-2} mbar. Thermal decomposition was achieved by slow heating in air up to 600ºC. The pure phases were obtained after repeated heatings at 850ºC (with intermediate grindings), each of 10 h, under nitrogen atmosphere. A flow chart for this method is shown in Figure 1d.

2.5 Characterization

Room temperature X-ray powder diffraction data were collected in the $18 \leq 2\theta \leq 110°$ range with an integration time of 10 s/0.02° step. A Bruker D8 Advance diffractometer equipped with a Cu tube, a Ge (111) incident beam monochromator (λ = 1.5406 Å) and a Sol-X energy dispersive detector were used for the samples obtained by glycine-nitrate route and LSSB-ss. A Philips X'Pert-MPD X-ray diffractometer with secondary beam graphite monochromated Cu–Kα radiation was used for the samples obtained by ceramic solid-state, sol-gel and freeze-drying techniques.

All samples were single phase without detectable impurities. The crystal structure was refined by the Rietveld method (Rietveld, 1959) from X-ray powder diffraction data using GSAS software package (Larson & Von Dreele, 1994).

Microstructural analysis was carried out in a JEOL JSM 6400 scanning electron microscope (SEM) using a secondary electron detector at 30 kV and 1.10^{-10} A for the LPS20, LNSC30, LPSC40, LPSC50, LPSC60, LPSC70 samples and a JEOL JSM-7000F at 3 kV and 11.10^{-12} A for the rest of samples.

3. Results

3.1 Characterization of $Ln_{1-x}A_xFeO_{3-\delta}$ (Ln=La, Nd, Pr; A=Sr, Ca) perovskites with 0.2≤x≤0.8

The $(La_{1-x}Sr_x)FeO_{3-\delta}$ (LSF) perovskite system exhibits high electronic and oxide ion conductivities at high temperatures, which make it attractive for solid oxide fuel cell (SOFC) cathodes. Several works (Ecija et al., 2011; Rodríguez-Martínez & Attfield, 1996; Vidal et al., 2007 and references therein) have shown that the physical properties of these perovskite materials are very sensitive to changes in the doping level (x) the average size of the A cations ($\langle r_A \rangle$) and the effects of A cation size disorder ($\sigma^2(r_A)$).

The synthesis of these compounds allows us to study the effect of the variation of the doping level x on the properties of the perovskites with general formula $Ln_{1-x}A_xFeO_{3-\delta}$ (Ln=La, Nd, Pr; A=Sr, Ca) applied as SOFC cathodes. This has been achieved by keeping constant both the average size ($\langle r_A \rangle$) and the size mismatch ($\sigma^2(r_A)$) to 1.22 Å and 0.003 Å^2, respectively.

For the preparation of this series the solid state reaction route has been chosen due to its simplicity to obtain perovskite phases in the same synthetic conditions.

3.1.1 Structural study

The room temperature X-ray powder diffraction patterns of these compounds are shown in Fig. 2a. A structural transition from orthorhombic symmetry (space group *Pnma*) for samples with x≤0.4 to rhombohedral symmetry (space group *R-3c)* for 0.5≤x≤ 0.7 compounds, and finally, to a mixture of rhombohedral *R-3c* and cubic *Pm-3m* perovskite phases for the x = 0.8 composition was observed. Representative Rietveld fits to the X-ray diffraction data for the samples LPS20, LNSC50 and LNSC80 are shown in Fig. 2b, 2c and 2d, respectively.

The dependence with the doping level x of the cell parameters and cell volume per formula unit and atomic distances and bond angles for all samples are represented in Figure 3a and b, respectively. There is a systematic decrease in volume, cell parameters and <Fe-O> distances with increasing doping level across the series. Given that in the system studied the A-site mean ionic radius $\langle r_A \rangle$ has been kept constant as the doping level increases, the observed effect can be solely associated to a reduction of the Fe-site mean ionic radius as it oxidises from Fe^{3+} to Fe^{4+}, with smaller radius ($\langle r_{Fe} \rangle$, $r_{Fe^{3+}}$=0.645 Å and $r_{Fe^{4+}}$ =0.585 Å) (Shannon, 1976). Details of these effects are given elsewhere (Vidal et al., 2007).

The increase of the <A-O> distances and <Fe-O-Fe> bond angles with increasing doping level (x) can be explained due to the structural transition produced with x: when passing from orthorhombic (*Pnma,* LPS20) to a mixture of rhombohedral and cubic (*R-3c* + *Pm-3m,* LSC80) the octahedra that compose the perovskite structure reduce its cooperative tilting and the structure "expands".

These results are in nice agreement with other structural studies of related perovskites in which similar structural transitions with doping level were observed (Blasco et al., 2008; Dann et al., 1994; Tai et al., 1995).

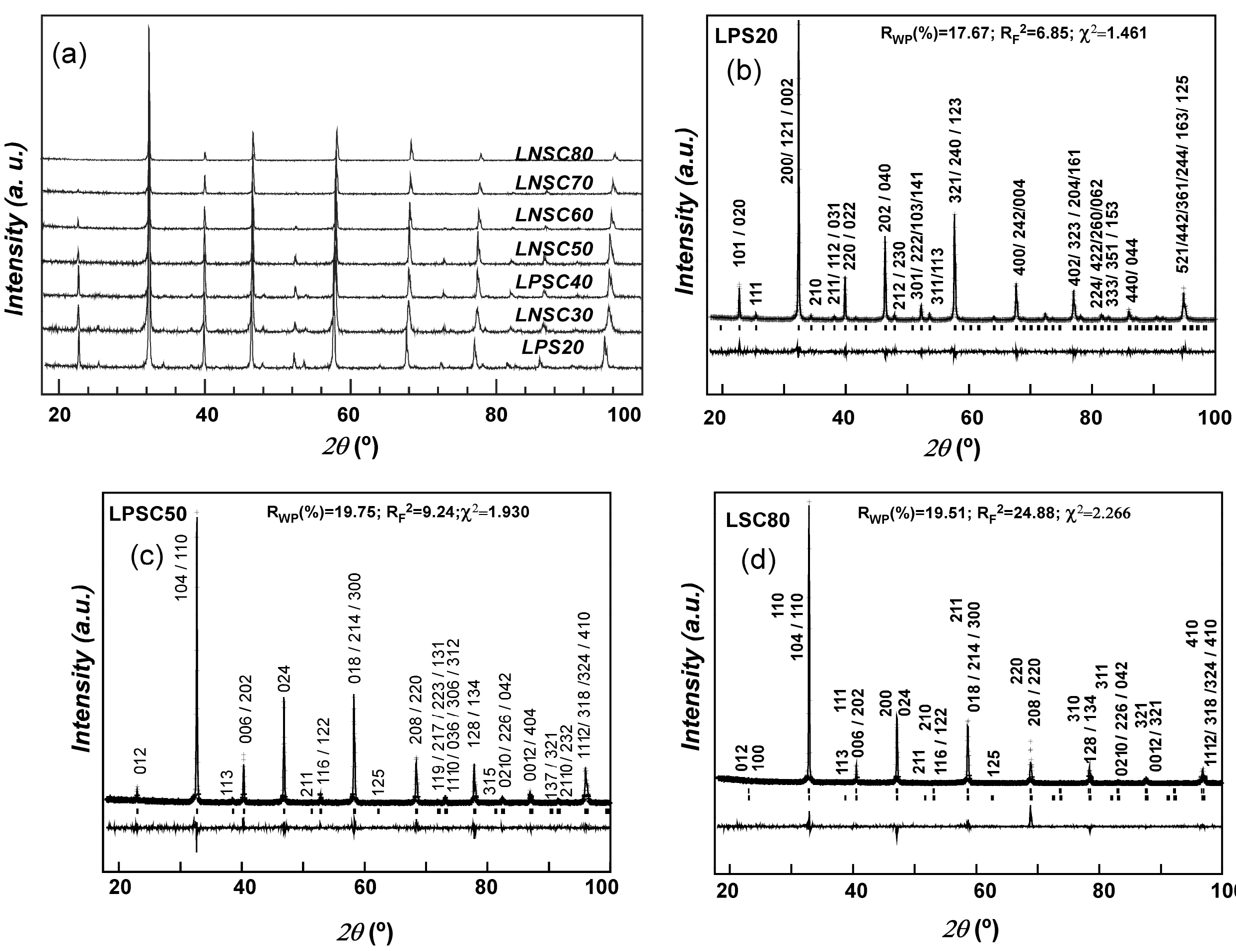

Fig. 2. (a) X-ray diffraction patterns for the series $Ln_{1-x}A_xFeO_{3-\delta}$ with x=0.2 to x=0.8, all obtained by the ceramic route. Rietveld fits to the X-ray diffraction data for samples LPS20 (b), LPSC50 (c) and LSC80 (d).

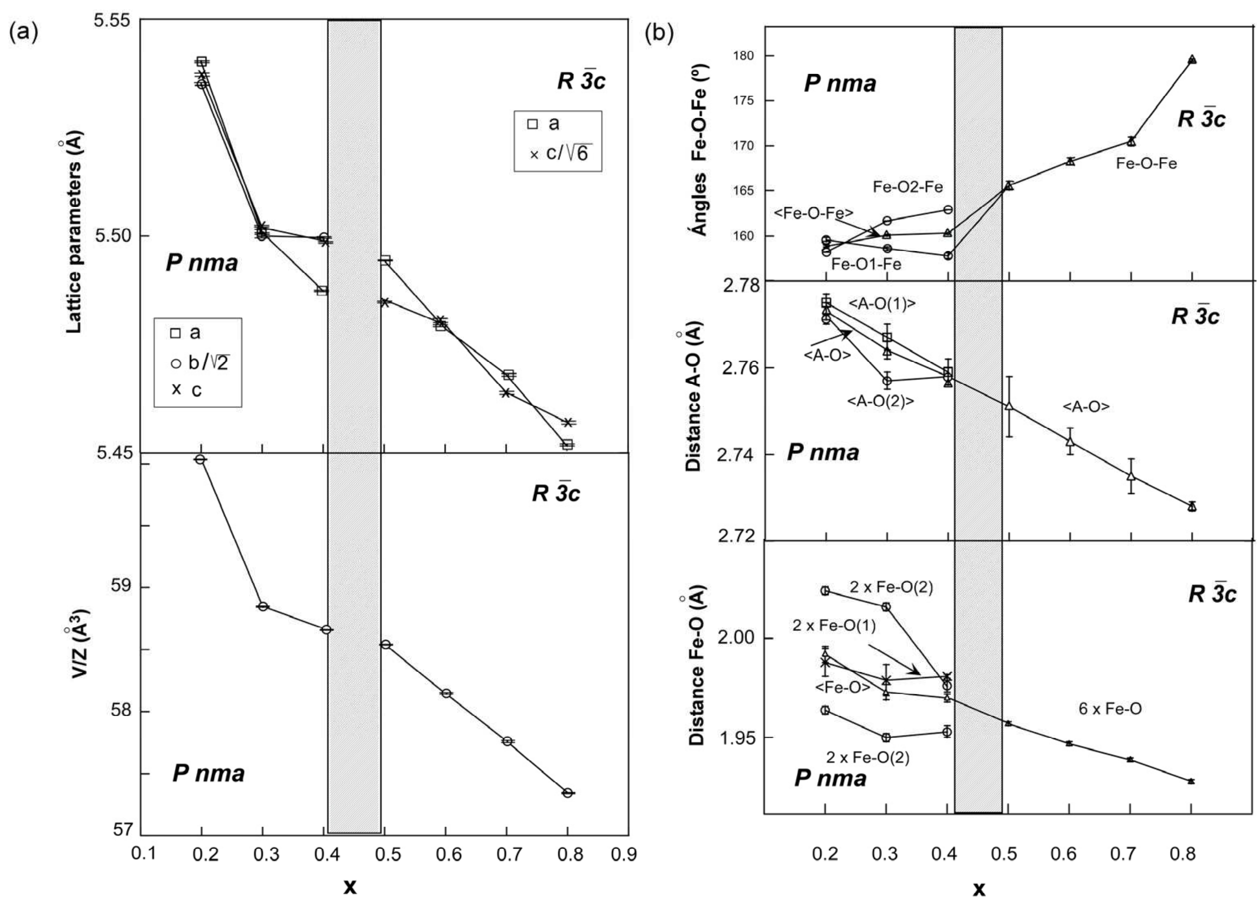

Fig. 3. (a) Variation of the unit cell parameters and volume per formula unit with doping, x. (b) Dependence of the mean atomic distances and bond angles with doping, x. Shaded area indicates the x range where the structural transition takes place.

3.1.2 Morphological study

Microstructure of bulk samples was study by scanning electron microscopy (SEM). Images of the sintered bars at 1300ºC are shown in Fig. 4.

These micrographs show different particle size distributions with grain sizes ranging between 0.33 and 2.83 µm for sample LPS20, to 5 and 37 µm for sample LSC70.

The dispersion in particle sizes is larger for values of x≥0.4. As observed previously (Liou, 2004a, 2004b) this increase in particle size with the doping level seems to be a result of a change in the melting point of the samples that decreases increasing alkaline-earth cation content. According to Kharton et al. (Kharton et al., 2002) this effect results in a liquid-phase assisted by sintering and an enhanced grain growth.

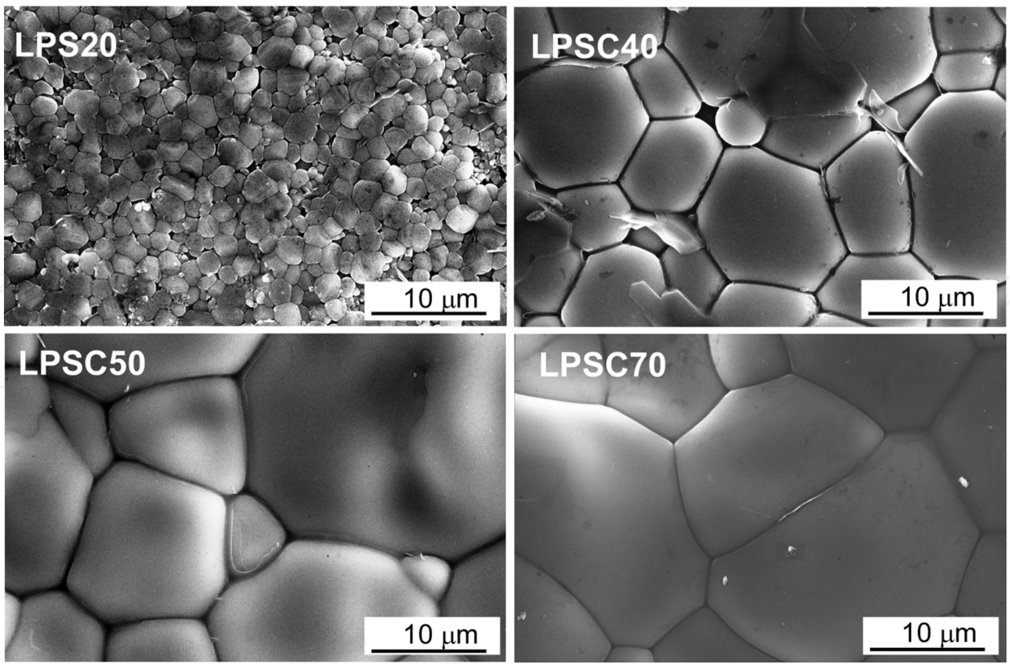

Fig. 4. (a) Scanning electron microscopy (SEM) images obtained at the same magnification for all $Ln_{1-x}A_xFeO_{3-\delta}$ compositions as a function of doping level x.

3.2 $Ln_{0.5}A_{0.5}FeO_{3-\delta}$ (Ln= La, Nd, Sm; A= Ba, Sr) 1.25≤ $\langle r_A \rangle$ ≤1.34 Å perovskites

As in the case of the previous family of iron perovskites, this new series of compounds are of interest for their use as mixed ionic electronic conducting materials, mainly from the point of view of cathodes for Solid Oxide Fuel Cells (SOFC), although they could also be used as ceramic membranes for oxygen separation. In the present case, the degree of lanthanide substitution was fixed to x=0.5 given that previous studies have shown that it is precisely at this degree of substitution when electronic and ionic conductivity are maximised (Hansen, 2010; Vidal et al., 2007).

In the present series of compounds the effect of the $\langle r_A \rangle$ variation on the properties of four different phases, $Ln_{0.5}A_{0.5}FeO_{3-\delta}$ (Ln=La, Nd, Sm; A=Ba, Sr) was evaluated. For this series (Table 1), $\langle r_A \rangle$ has been varied between 1.34 and 1.25 Å keeping x and $\sigma^2(r_A)$ constant, with values of 0.5 and 0.0161 Å^2, respectively.

Prior to choosing a synthesis method for all samples, two different methods were tried for one of the samples, $La_{0.05}Sm_{0.45}Sr_{0.18}Ba_{0.32}FeO_{3-\delta}$, for which the structural parameters and morphology were evaluated. The ceramic and glycine-nitrate routes were used in the present case.

3.2.1 Influence of the synthetic method on the structure and morphology of the $La_{0.05}Sm_{0.45}Sr_{0.18}Ba_{0.32}FeO_{3-\delta}$

Laboratory X-ray diffraction data at room temperature for $La_{0.05}Sm_{0.45}Ba_{0.5}FeO_{3-\delta}$ obtained by ceramic and glycine-nitrate routes were extremely similar, both samples being pure to the detection limits of the technique. XRD patterns were fitted by the Rietveld method (Figure 5) considering a rhombohedral symmetry (space group *R*-3*c*) in both cases.

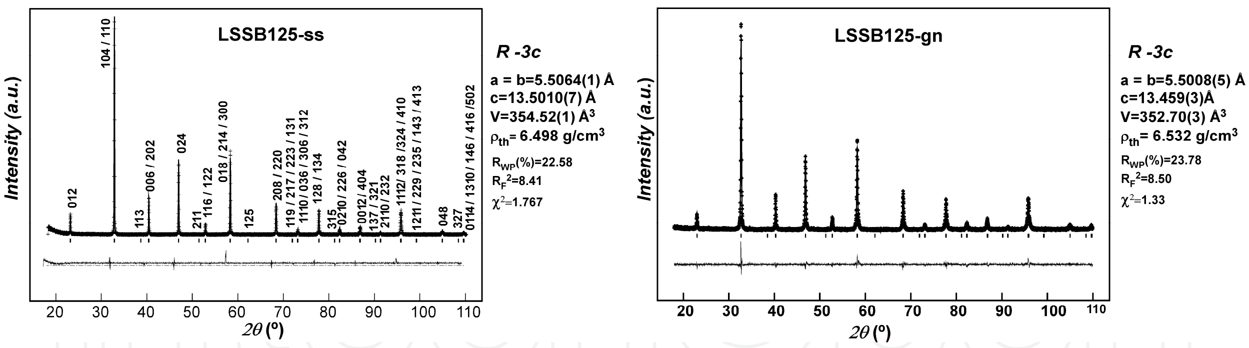

Fig. 5. Rietveld fits to room XRD patterns for LSSB-ss and LSSB-gn samples. In each case, lattice parameters (a, b, c), unit cell volume (V) and theoretical density (ρ) are included.

From the fits to the XRD data it was observed that both phases are nearly identical: they crystallise in the same space group and does not show significant difference among lattice parameters, cell volume or density values.

The morphological study, however, shows a different picture. As shown in Figure 6, where SEM micrographs taken at the same amplification for both samples are presented, their microstructure is quite different. The sample prepared following the ceramic route presents a microstructure with heterogeneous grain sizes and shapes, in which particles range from ~ 2 to approximately 8 μm in diameter. On the other hand, the average grain size of the sample obtained by glycine-nitrate route is about 200 nm, almost an order of magnitude smaller. The higher calcination temperature and longer reaction time required to obtain the samples in the ceramic process can explain the bigger grain size showed for these samples (Melo Jorge et al., 2001).

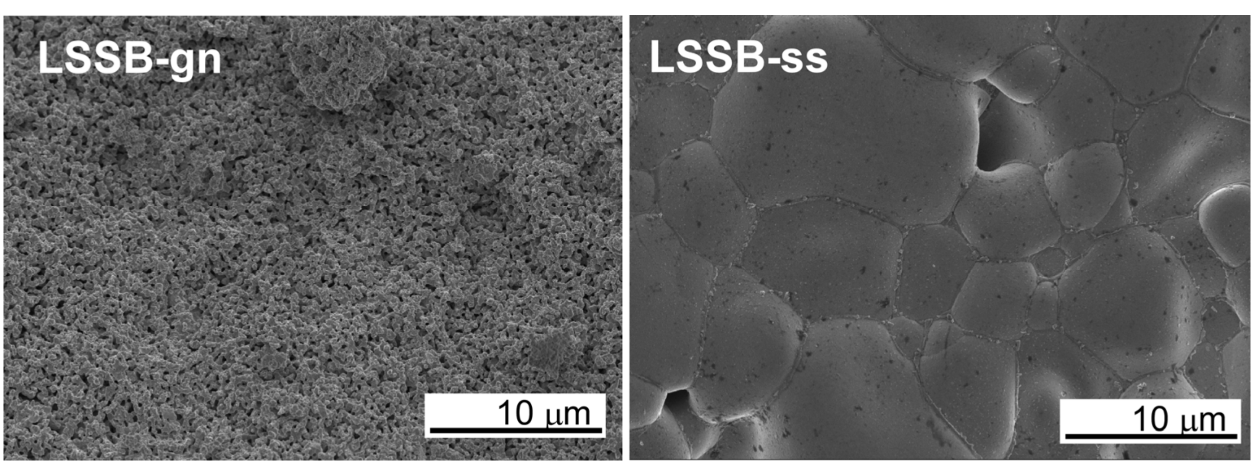

Fig. 6. SEM micrographs taken on the surface of the $La_{0.05}Sm_{0.45}Sr_{0.18}Ba_{0.32}FeO_{3-\delta}$ phases obtained by the glycine-nitrate (gn) and solid state reaction (ss) methods.

For the application as SOFC cathodes, samples with small and homogeneous particle sizes are usually preferred. As a consequence, the glycine-nitrate process was considered a more appropriate technique for preparing the perovskite samples of this series: $Ln_{0.5}A_{0.5}FeO_{3-\delta}$ (Ln= La, Nd, Sm; A= Ba, Sr) with 1.25≤ $\langle r_A \rangle$ ≤1.34 Å.

3.2.2 Structural study

Room temperature X-ray diffraction patterns of the LB134, LNSB131, LNSB128, LSSB125-gn samples show that all the samples are single phase compounds (Figure 7a). A shift of the diffraction maxima to lower diffraction angles (2θ) with decreasing <r_A> anticipates an increase of the lattice parameters. X-ray powder diffraction patterns were indexed using a cubic symmetry (*Pm-3m* space group) for the LB134 and LNSB131 samples and a rhombohedral symmetry (*R-3c* space group) in the case of LNSB128 and LSSB125-gn compounds. Figure 7b shows the Rietveld fits to the XRD patterns for two samples.

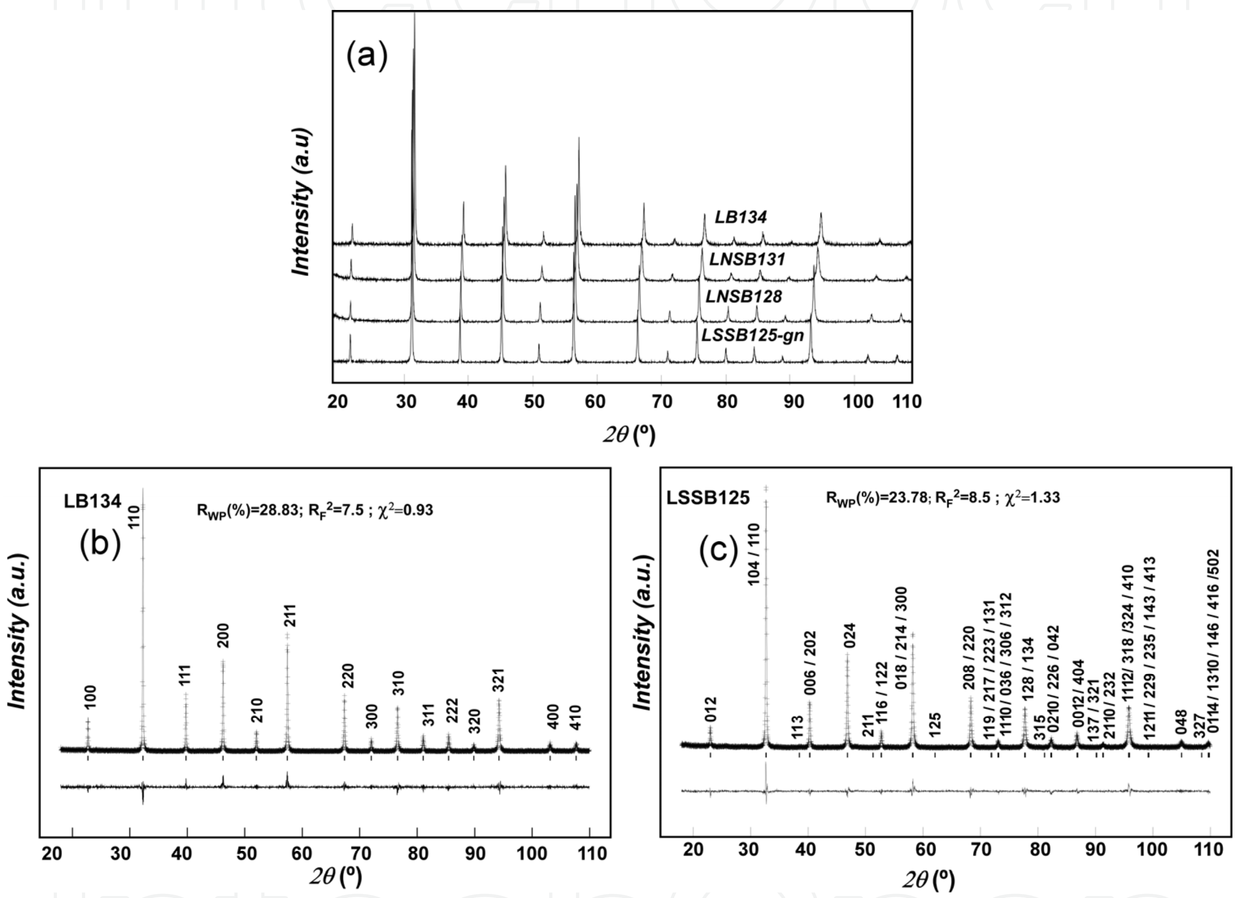

Fig. 7. (a) X-ray powder diffraction patterns at room temperature for all samples. (b) and (c) show the Rietveld fits to the X-ray powder diffraction patterns at room temperature for LB134-ss and LSS125-ss samples.

The <r_A> dependence of the lattice parameters, unit cell volume, main bond distances and Fe-O-Fe bond angles are shown in Figure 8. As it can be observed, lattice parameters and unit cell volume decrease with decreasing the average A-site ionic radius. Given that the doping level has been fixed (x=0.5), changes in the ratio Fe^{3+}/Fe^{4+} and, therefore, in the Fe-site ionic radius (<r_{Fe}>), are not expected. Consequently, the decrease in lattice parameters is ascribed to the variation of <r_A>. A more detailed analysis is given elsewhere (Ecija et. al, 2011). This also explains the decrease of the <A-O> and <A-Fe> mean distances with decreasing <r_A> (Figure 8b). Although <r_{Fe}> has been kept constant, there is a slight reduction of the <Fe-O> distances as <r_A> decreases, which is a consequence of the tilting in the FeO_6 octahedra due to the rhombohedral distortion. The decrease of the <Fe-O-Fe> bond angles is the result of the same effect (Woodward, 1998).

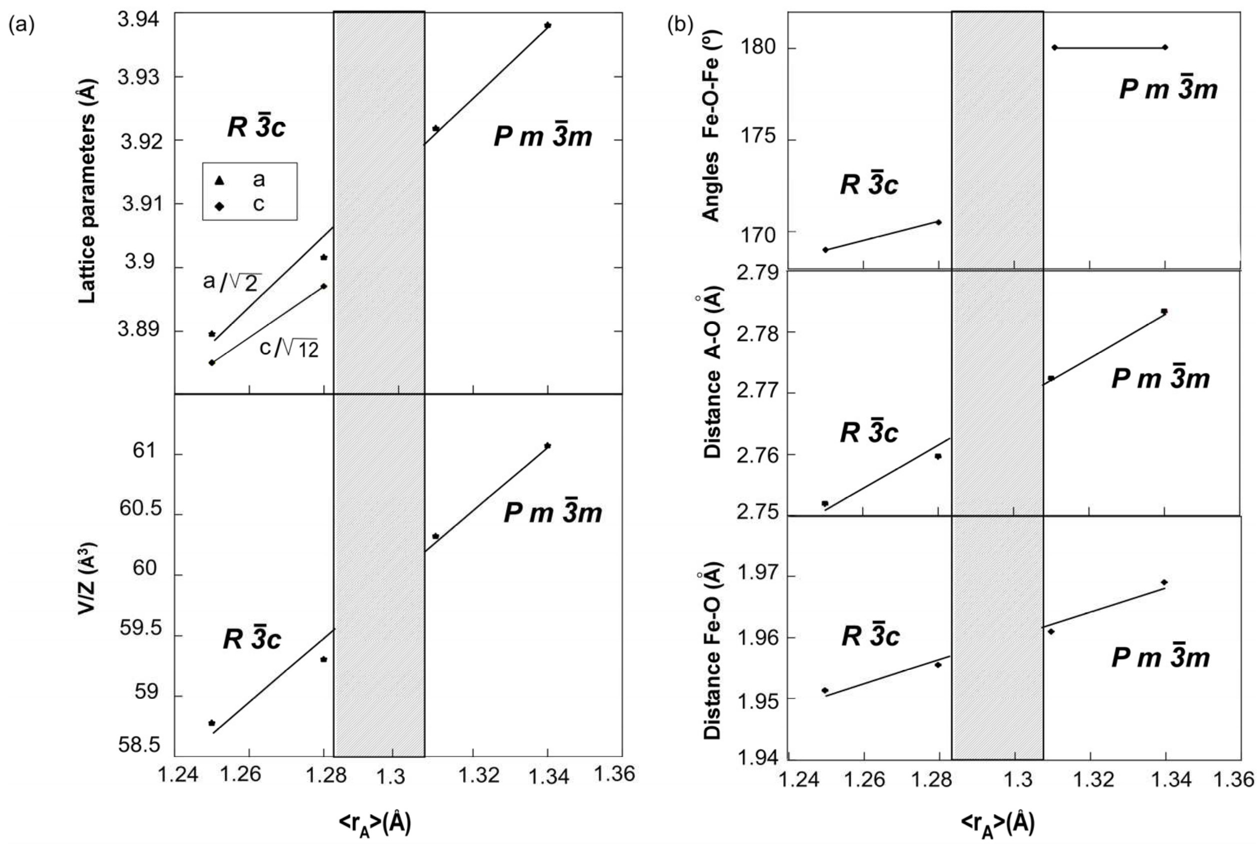

Fig. 8. $<r_A>$ dependence of (a) the unit cell parameters and volume per formula unit; and (b) the main average bond lengths (<A–Fe>, <A–O>, <Fe–O>) and Fe–O–Fe bond angle. Shaded area indicates the x range where the structural transition takes place.

3.2.3 Morphological study

Figure 9 shows the SEM micrographs of the LB134, LNSB131, LNSB128, LNSB125-gn bulk samples after the last heating at 1050ºC.

In this series of samples no significant differences can be found in the morphology and average particle size. All samples present some agglomeration and fine grain size. Image analysis of the micrographs has allowed us to determine that the average grain size of the samples is in the range of 150-250 nm.

3.3 Synthesis and characterization of $Nd_{0.8}Sr_{0.2}(Mn_{1-x}Co_x)O_3$ perovskites with x = 0.1, 0.2, 0.3

The hole-doped perovskite manganese oxides with general formula $Ln_{1-x}A_xMnO_3$ (Ln= La, Pr, Nd; A= Ca, Sr, Ba, Pb; x<0.5) draw considerable attention in the late 1990´s due to their colossal magneto-resistance (CMR) effect at low temperatures (Rao, 1998). In the search for new CMR materials it was observed that doping on Mn site by other transition metal elements, such as Cr, Fe, Co and Ni, was an effective way to obtain new materials, which also helped to understand the new phenomenon (Tai, 2000; Takeuchi, 2002; Ulyanov, 2007). Phase morphology, highly dependent on preparative conditions, was also observed to play an important role in the effect: low temperature CMR was improved as the grain size was reduced (Das, 2002). In order to help in this area, it was decided to study the effects of the synthesis method in a series of perovskite compounds with the general formula $Nd_{0.8}Sr_{0.2}(Mn_{1-x}Co_x)O_3$ ($0.1 \le x \le 0.3$). The sol-gel and freeze-drying techniques were used in order to compare their structural, morphological and magnetic properties. Details of the later (magnetic properties) can be found elsewhere (Vidal et al., 2005).

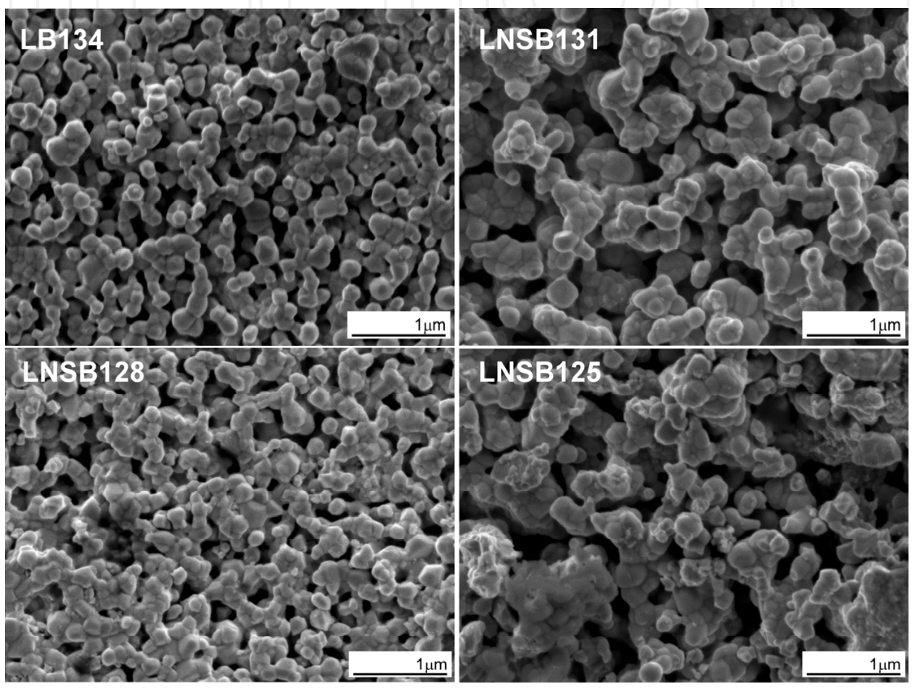

Fig. 9. SEM micrographs of the surface of the LB134, LNSB131, LNSB128, LSSB125-gn bulk samples.

3.3.1 Structural study

The X-ray powder diffraction patterns (XRPD) of all the compounds studied in this section were indexed in the orthorhombic space group *Pmna* irrespective of the synthesis method used. Fig. 10 shows the XRD and Rietveld refinement profiles for all phases with the formula $Nd_{0.8}Sr_{0.2}(Mn_{1-x}Co_x)O_3$.

When the lattice parameters and cell volume are compared a slight decrease with increasing cobalt content is observed in both cases. This effect is related to the changes in sizes of the B site atoms upon doping (Meera et al., 2001; Pollert et al., 2003). The oxidation states of Mn and Co in the $AMn_{1-x}Co_xO_3$ systems has been for long debated (Goodenough et al., 1961; 1997; Toulemonde et al., 1998; Troyanchuk et al., 2000), and different mixtures of Mn^{4+}-Mn^{3+} and Co^{3+}-Co^{2+} have been proposed. The most likely combination, based in spectroscopic and magnetic results, seems to indicate that the cobalt is introduced as Co^{2+} (and not as Co^{3+}) thus causing a mixed state (4+ and 3+) in manganese. This mixture of oxidation states has also been proved useful for Pollert et al. to explain magnetic and electrical properties of the series $Nd_{0.8}Na_{0.2}Mn_{1-x}Co_xO_3$ ($x \le 0.1$), $Pr_{0.8}Na_{0.2}Mn_{1-x}Co_xO_3$ ($x \le 0.2$) (Pollert et al., 2003a, 2003b) and $La_{0.8}Na_{0.2}Mn_{1-x}Co_xO_3$ ($x \leq 0.2$) (Pollert et al., 2004). On the other hand, as the Co content increases, the LSMC materials would shift from the oxygen excessive region to the oxygen deficient region, which would also contribute to the decrease in the unit volume. Wandekar et al. (Wandekar et al., 2009) carried out a detailed study on the crystal structure and conductivity of Co substituted LSM system and showed that the change in the ion radius of B-site element plays a predominant role at low Co content and the increase in oxygen vacancy becomes dominant at high Co content.

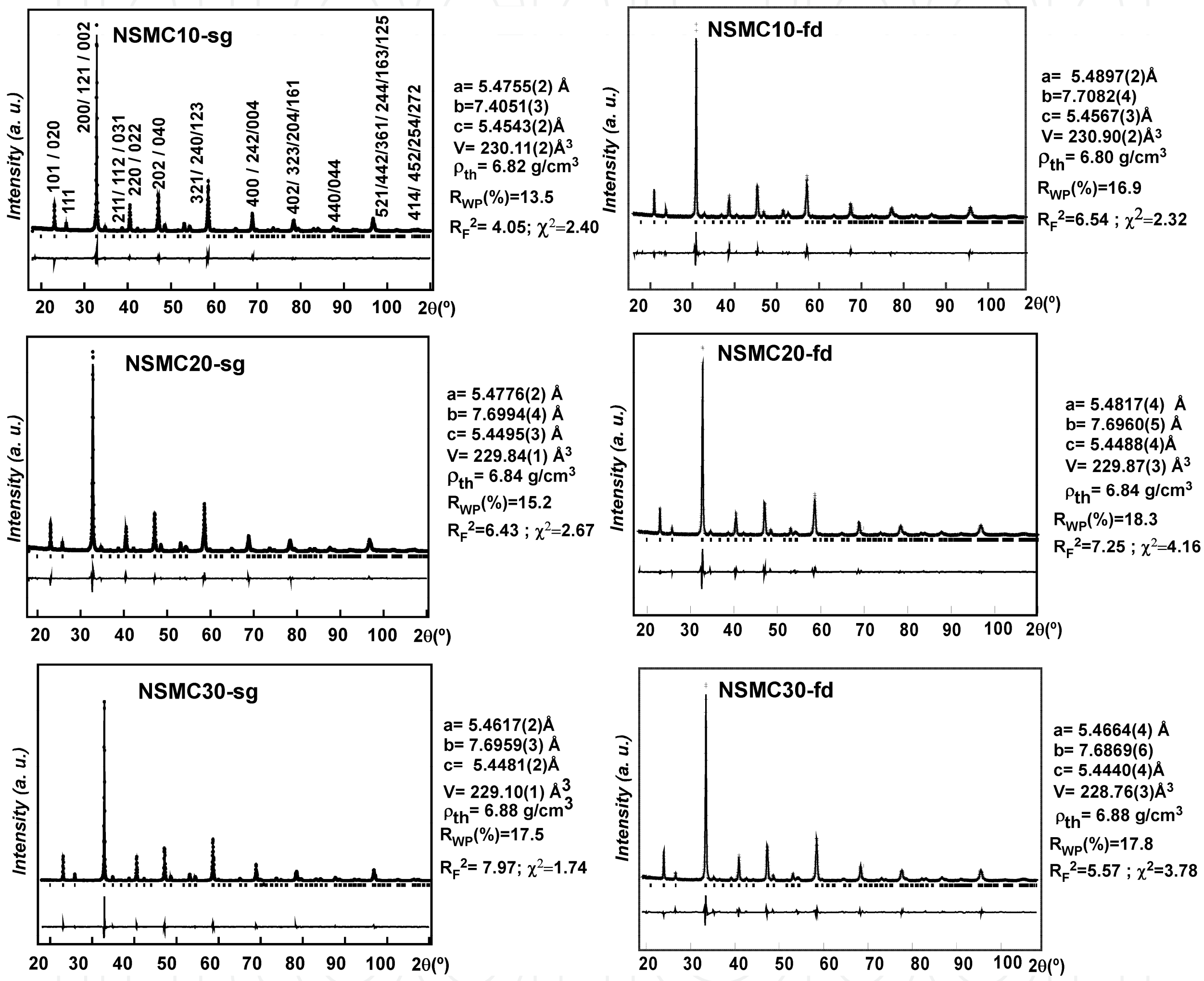

Fig. 10. Rietveld fits to the X-ray diffraction data in the orthorhombic *Pnma* space group for the $Nd_{0.8}Sr_{0.2}Mn_{1-x}Co_xO_3$ compounds. The labels "sg" and "fd" indicates that samples were prepared using the sol gel and freeze-drying techniques, respectively. In each case, lattice parameters (a, b, c), unit cell volume (V) and theoretical density (ρ) data are inset.

In consequence, considering only the high spin states of these elements and assuming nearly oxygen stoichiometric phases at room temperature, the observed reduction of the lattice volume in the present samples is consistent with the gradual appearance of Mn^{4+} (of smaller size than Mn^{3+} and Co^{2+} (Shannon, 1976) and so with the reduction of the mean B-site ionic radii. This explanation is also satisfactory for the same effect in the compounds $La_{0.7}Na_{0.3}Mn_{1-x}Co_xO_3$ where the authors had assumed the presence of only Mn^{3+}–Co^{3+} (Meera et al., 2001).

Table 2 shows details of the averge interatomic <B-O>, <A-O> and <A-B> distances together with <B-O-B> bond angles. As it can be observed <B-O> and <A-B> distances decrease as the cobalt concentration increases. These tendencies can be explained following the same reasoning indicated before, which basically concludes that cobalt enters in the structure in an oxidation state with smaller radius than manganese. No significant changes are observed in the <A-O> distances or in the <B-O-B> angles. This indicates that, despite the observed changes in the B size, the cobalt doping does not cause a noticeable distortion in the perovskite structure.

Variables		NSMC10		NSMC20		NSMC30	
		sg	fd	sg	fd	sg	fd
distance (Å)	<A–B>	3.346	3.350	3.345	3.345	3.341	3.339(1)
	<A–O1>	2.749(1)	2.756(1)	2.748(1)	2.751(2)	2.748(1)	2.747(2)
	<A–O2>	2.588(1)	2.592(1)	2.588(2)	2.593(2)	2.587(1)	2.591(2)
	<A–O>	2.668	2.674	2.668	2.672	2.667	2.671
	<B–O1>	1.954(4)	1.959(4)	1.950(4)	1.958(6)	1.958(4)	1.957(4)
	<B–O2>	1.968(1)	1.970(2)	1.967(2)	1.965(2)	1.963(2)	1.960(2)
	<B–O>	1.961	1.964	1.958	1.961	1.957	1.958
bond angle (°)	B-O1-B	160.8(4)	159.3(2)	161.5(4)	158.6(2)	158.5(3)	158.3(2)
	B-O2-B	157.9(4)	158.3(4)	158.2(4)	159.0(1)	158.5(3)	159.4(1)
	<B–O–B>	159.3	158.8	159.8	158.8	158.5	158.8

Table 2. Mean atomic distances and bond angles for the series of ABO_3 (A = $Nd_{0.8}$ $Sr_{0.2}$; B = $Mn_{1-x}Co_x$; x = 0.1, 0.2 and 0.3) samples prepared by the two methods described in the text.

In the same way, no significant changes are observed between the compounds synthesised by the sol-gel or the freeze-drying techniques.

3.3.2 Morphological study

The SEM micrographs of the present series of compounds are shown in Fig. 11. All pictures were taken on sintered bars after they were prepared by the sol-gel and freeze-drying methods.

As observed, the $Nd_{0.8}Sr_{0.2}(Mn_{1-x}Co_x)O_3$ samples prepared by the sol-gel route show a homogeneous particle size morphology distributed in small agglomerates. The grain size of the nearly spherical particles decreases with Co content from ~ 200 nm for the sample with x = 0.1 to ~ 100 nm for x = 0.3. In the case of the compounds obtained by the freeze-drying technique the morphology of the particles is also spherical and homogeneous but the grain size is quite stable in all phases and slightly higher (~250 nm) than in the previous case.

According to some studies (Kuharuangrong et al., 2004), Co doping of 20% does not usually influence the grain size of LSM, but 40 % mol Co significantly reduces the grain size (about 5-10 μm) of the $La_{0.84}Sr_{0.16}Mn_{1-x}Co_xO_3$ (x= 0, 0.2, 0.4) samples prepared by conventional oxide mixing process. However, some reduction in the particle size was observed in the case of $La_{0.67}Pb_{0.33}Mn_{1-x}Co_xO_3$ (x= 0 and 0.3) compounds, which were also prepared by the ceramic route (Dhahri et al., 2010). The present observation of a reduction in the particle size of the $Nd_{0.8}Sr_{0.2}(Mn_{1-x}Co_x)O_3$ phases in one of the methods but not in the other would point towards the synthesis method as the responsible for this effect, rather than the amount of cobalt. In this case, however, the observed decrease of the grain size is less significant than in previous studies.

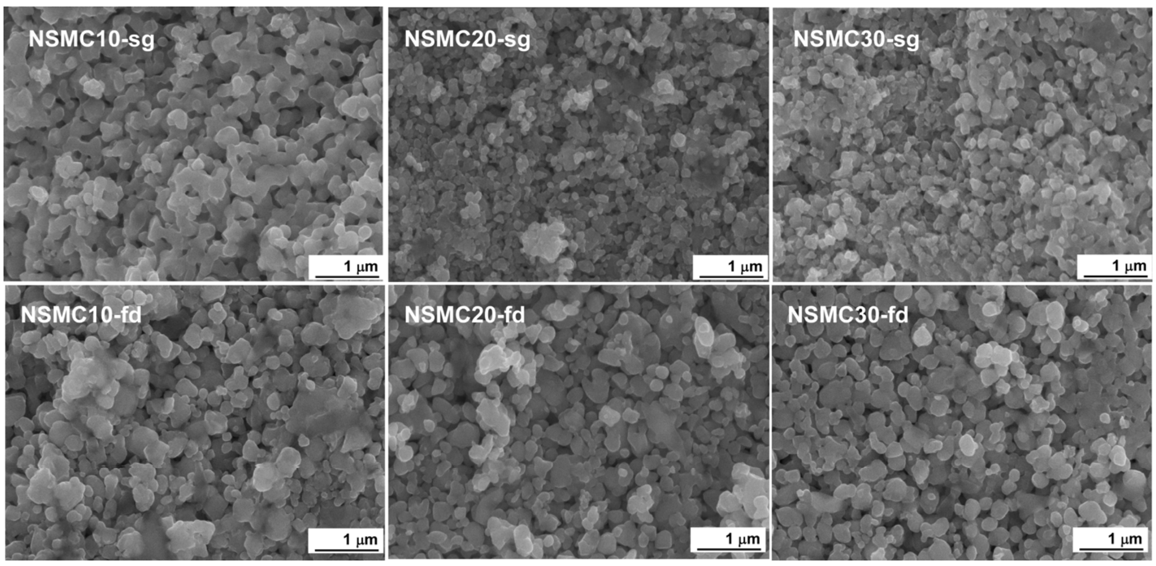

Fig. 11. Secondary electron SEM micrographs obtained for all $Nd_{0.8}Sr_{0.2}(Mn_{1-x}Co_x)O_3$ compositions prepared by (a) sol-gel (sg) and (b) freeze-drying (fd) methods.

4. Conclusion

Different synthetic methods were used to prepare several perovskite type compounds. Phase-pure perovskites were obtained in all cases, irrespective of the method of synthesis and even when more than one method was used. It is to note that no differences in the overall crystal structure were observed in any of the cases when the method was changed. Moreover, changes in the crystal structure of the compounds within each series could be perfectly explained considering only compositional (and resulting structural) variables such as the mean A-site ionic radius or the A-site disorder, none of them being influenced by the synthesis route. This is true for the $Ln_{1-x}A_xFeO_{3-\delta}$ series where changes from orthorhombic to cubic are consistent with the change in the doping level x and also for the $Ln_{0.5}A_{0.5}FeO_3$ where the change was observed from rhombohedral to cubic symmetry when the mean A-site radius, $\langle r_A \rangle$, was varied.

At least in the present group of compounds this seems to indicate that, properly used, and with no other factors present (such as in the case of the growth of samples on crystallographycally oriented substrates), the structural characteristics can be studied and properly addressed without having into account the synthesis method.

It is no news that, compared with the solid state reaction, the glycine-nitrate route, sol-gel and freeze-drying techniques require lower calcination temperatures to yield pure crystals of perovskite phases, with the resulting energy saving (very important nowadays). The disadvantage is, however, the fact that they are more time consuming and require more controlled synthesis conditions. In the same way, it is clearly observed that the ceramic method always yields phases with higher particle sizes but this is not a disadvantage if the final compounds are not to be used in an application that requires high specific area. It is to note that in the case of the $Nd_{0.8}Sr_{0.2}(Mn_{1-x}Co_x)O_3$, grain size was observed to change depending on the synthesis route. Although no significant differences were observed in the crystal structure, sol-gel method resulted in smaller grain sizes than the freeze drying method. In consequence, this seems to be a consequence of the preparative method which reinforces the idea that, if the microstructure of the sample is the key issue, the use of several synthesis methods is always worth trying.

5. Acknowledgments

This work has been financially supported by the Ministerio de Ciencia e Innovación PSE-12000-2009-7 (MICINN) and MAT 2010-15375; Consejería de Industria, Innovación, Comercio y Turismo (SAIOTEK 2011) and by the Consejería de Educación, Universidades e Investigación (IT-177-07) of the Basque Goverment of Gobierno Vasco/Eusko Jaurlaritza. Technical and human support provided by SGIker (UPV/EHU, MICINN, GV, EJ, ESF) and Alternative Generation Systems Group of Technological Research Centre is gratefully acknowledged.

6. References

Bansal, N.P. & Zhong, Z. (2006). Combustion Synthesis of $Sm_{0.5}Sr_{0.5}CoO_{3-x}$ and $La_{0.6}Sr_{0.4}CoO_{3-x}$ Nanopowders for Solid Oxide Fuel Cell Cathodes. *Journal of Power Sources*, Vol. 158, No. 1, (July 2006), pp. 148-153, ISSN: 0378-7753

Bell, R.J.; Millar, G.J. & Drennan. (2000). J. Influence of Synthesis Route on the Catalytic Properties of $La_{1-x}Sr_xMnO_3$. *Solid State Ionics,* (June 2000), Vol. 131, No. 3, 4, pp. 211-220, ISSN: 0167-2738

Berger, D.; Matei, C.; Papa, F.; Macovei, D.; Fruth, V. & Deloume, J.P. (2007). Pure and Doped Lanthanum Manganites Obtained by Combustion Method. *Journal of the European Ceramic Society*, Vol. 27, No. 13-15, (March 2007), pp. 4395-4398, ISSN: 0955-2219

Blasco, J.; Aznar, B.; García, J.; Subías, G.; Herrero-Martín, J. & Stankiewicz, J. (2008). Charge Disproportionation in $La_{1-X}Sr_XFeo_3$ Probed by Diffraction and Spectroscopic Experiments. *Physical Review B*, Vol. 77, Nº 5, (February 2008), pp. 054107-1-054107-10, ISSN: 1098-0121

Carp, O.; Patron, L.; Ianculescu, A.; Pasuk, J. & Olar, R. (2003). New Synthesis Routes for Obtaining Dysprosium Manganese Perovskites. *Journal of Alloys and Compounds*, Vol. 351, No. 1-2, (March 2003), pp. 314-318, ISSN: 0925-8388

Cheetham, A.K. & Day, P. (1987). *Solid State Chemistry: Techniques*, Oxford University Press, ISBN: 0198551657, Oxford

da Conceicao, L.; Silva, C.R.B.; Ribeiro, N.F.P. & Souza, M.M.V.M. (2009). Influence of the Synthesis Method on the Porosity, Microstructure and Electrical Properties of $La_{0.7}Sr_{0.3}MnO_3$ Cathode Materials. *Materials Characterization*, Vol. 60, No. 12, (December 2009), pp. 1417-1423, ISSN: 1044-5803

Dann, S.E; Currie, D.B.; Weller, M.T.; Thomas, M.F. & Al-Rawwas, A.D. (1994). The Effect of Oxygen Stoichiometry on Phase Relations and Structure in the System $La_{1-x}Sr_xFeO_{3-\delta}$ ($0 \leq x \leq 1$, $0 \leq \delta \leq 0.5$). *Journal of Solid State Chemistry*, Vol. 109, No. 1, (March 1994), pp. 134-144, ISSN: 0022-4596

Das, S.; Chowdhury, P.; Gundu Rao, T. K.; Das, D. & Bahadur, D. (2002). Influence of Grain Size and Grain Boundaries on the Properties of $La_{0.7}Sr_{0.3}Co_xMn_{1-x}O_3$. *Solid State Communications*, Vol. 121, No. 12, (March 2002), pp. 691-695, ISSN: 0038-1098

Dhahri, N.; Dhahri, A.; Cherif, K.; Dhahri, J.; Taibi, K. & Dhahri, E. Structural, Magnetic and Electrical properties of $La_{0.67}Pb_{0.33}Mn_{1-x}Co_xO_3$ ($0 \leq x \leq 0.3$). *Journal of Alloys and Compounds*, Vol. 496, No. 1-2, (October 2010), pp. 69-74, ISSN: 0925-8388

Dho, J.; Leung, C.W.; MacManus-Driscoll, J.L. & Blamire, M.G. (2004). Epitaxial and Oriented $YMnO_3$ Film Growth by Pulsed Laser Deposition. *Journal of Crystal Growth*, Vol. 267, No. 3-4, (July 2004), pp. 548-553, ISSN: 0022-0248

Dutta, A.; Mukhopadhyay, J. & Basu, R.N. (2009). Combustion Synthesis and Characterization of LSCF-based Materials as Cathode of Intermediate Temperature Solid Oxide Fuel Cells. *Journal of the European Ceramic Society*, Vol. 29, No.10, (July 2009), pp. 2003-2011, ISSN: 0955-2219

Ecija, A.; Vidal, K.; Larrañaga, A.; Martínez-Amesti, A.; Ortega-San-Martín, L. & Arriortua, M.I. (2011). Characterization of $Ln_{0.5}M_{0.5}FeO_{3-\delta}$ (Ln=La, Nd, Sm; M=Ba, Sr) Perovskites as SOFC Cathodes. *Solid State Ionics*, Vol. 201, No. 1, (October 2011), pp. 35-41, ISSN: 0167-2738

Fukuoka, H.; Isami, T. & Yamanaka, S. (1997). Superconductivity of Alkali Metal Intercalated Niobate with a Layered Perovskite Structure. *Chemistry Letters*, Vol. 8, (April 1997), pp. 703-704, ISSN: 0366-7022

Goodenough, J.B.; Wold, A.; Wold, R.J.; Arnott, R.J. & Menyuk, N. (1961). Relationship Between Crystal Symmetry and Magnetic Properties of Ionic Compounds Containing Mn^{3+}. *Physical Review*, Vol. 124, (October 1961), pp. 373-384, ISSN: 0031-899X

Hansen, K.K. (2010). Electrochemical Reduction of Nitrous Oxide on $La_{1-x}Sr_xFeO_3$ Perovskites. *Materials Research Bulletin*, Vol. 45, No. 9, (May 2010), pp. 1334-1337, ISSN: 0025-5408

Inaguma, Y.; Liquan, C.; Itoh, M.; Nakamura, T.; Uchida, T.; Ikuta, H. & Wakihara, M. (1993) High Ionic Conductivity in Lithium Lanthanum Titanate. *Solid State Communications*, Vol. 86, No. 10, (June 1993), pp. 689-693, ISSN: 0038-1098

Kakihana, M. & Yoshimura, M. (1999). Synthesis and Characteristics of Complex Multicomponent Oxides Prepared by Polymer Complex Method. *Bulletin of the Chemical Society of Japan*, Vol. 72, No. 7, (1999), pp. 1427-1443, ISSN: 0009-2673

Kharton, V.V.; Shaulo, A.L.; Viskup, A.P.; Avdeev, M.; Yaremchenko, A.A.; Patrakeev, M.V.; Kurbakov, A.I.; Naumovich, E.N. & Marques, F.M.B. (2002). Perovskite-like System $(Sr,La)(Fe,Ga)O_{3-\delta}$: Structure and Ionic Transport under Oxidizing Conditions. *Solid State Ionics*, Vol. 150, No. 3-4, (October 2002), pp. 229-243, ISSN: 0167-2738

Kuharuangrong, S.; Dechakupt, T. & Aungkavattana, P. (2004). Effects of Co and Fe Addition on the Properties of Lanthanum Strontium Manganite. *Materials Letters*, Vol. 58, No. 12-13, (May 2004), pp. 1964-1970, ISSN: 0167-577X

Larson, A.C. & Von Dreele R.B. (1994). *GSAS: General Structure Analysis System, LAUR*, pp. 86–748

Liang, J.J. & Weng, H.S. (1993). Catalytic Properties of Lanthanum Strontium Transition Metal Oxides ($La_{1-x}Sr_xBO_3$; B = Manganese, Iron, Cobalt, Nickel) for Toluene Oxidation. *Industrial & Engineering Chemistry Research*, Vol. 32, No. 11, (November 1993), pp. 2563-2572, ISSN: 0888-5885

Liou, Y.C. (2004). Effect of Strontium Content on Microstructure in $(La_xSr_{1-x})FeO_3$ Ceramics. *Ceramics International*, Vol. 30, No. 5, (March 2004), pp. 667-669, ISSN: 0272-8842

Liou, Y.C. (2004). Microstructure Development in $(La_xSr_{1-x})MnO_3$ Ceramics. *Materials Science & Engineering, B*: *Solid-State Materials Advance Technology*, Vol. 108, No. 3, (April 2004), pp. 278-280, ISSN: 0921-5107

Liu, B. & Zhang, Y. (2008). $Ba_{0.5}Sr_{0.5}Co_{0.8}Fe_{0.2}O_3$ Nanopowders Prepared by Glycine-nitrate Process for Solid Oxide Fuel Cell Cathode. *Journal of Alloys and Compounds*, Vol. 453, No. (1-2), (April 2008), pp. 418-422, ISSN: 0925-8388

Meera, K.V.K.; Ravindranayh, V. & Rao M.S.R. (2001). Magnetotransport Studies in $La_{0.7}Ca_{0.3}Mn_{1-x}M_xO_3$ (M = Co, Ga). *Journal of Alloys and Compounds*, Vol. 326, No. 1-2, (August 2001), pp. 98-100, ISSN: 0925-8388

Melo Jorge, M.E.; Correia dos Santos, A. & Nunes, M.R. (2001). Effects of Synthesis Method on Stoichiometry, Structure and Electrical Conductivity of $CaMnO_{3-\delta}$. *International. Journal of Inorganic Materials*, Vol. 3, No. 7, (November, 2001), pp. 915-921, ISSN: 14666049

Narlikar, A. (2001). Essential Chemistry of High-Tc Cuprate Synthesis through the Solution Precursor Methods, In: *Studies of High Temperature Superconductors*, Nova Science Publishers, New York, ISBN: 1-59033-026-9

Patil, K. C.; Aruna, S. T. & Mimani, T. (2002). Combustion Synthesis: an Update. *Current Opinion in Solid State & Materials Science*, Vol. 6, No. 6, (December 2002), pp. 507-512, ISSN: 1359-0286

Pithan, C., Hennings, D. & Waser, R. (2005). Progress in the Synthesis of Nanocrystalline $BaTiO_3$ Powders for MLCC, *International Journal of Applied Ceramic Technology*, Vol. 2, No. 1, (January 2005), pp. 1–14, ISSN: 1546-542X

Polini, R.; Pamio A. & Traversa. E. (2004). Effect of Synthetic Route on Sintering Behavior, Phase Purity and Conductivity of Sr- and Mg-doped $LaGaO_3$ Perovskites. *Journal of the European Ceramic Society*, Vol. 24, No. 6, (June 2004), pp. 1365-1370. ISSN: 0955-2219

Pollert, E.; Hejtmánek, J. ; Knížek, K.; Maryško M.; Doumerc, J.P.; Grenier J.C. & Etourneau, J. (2003). Insulator-metal Transition in $Nd_{0.8}Na_{0.2}Mn_{(1-x)}Co_xO_3$ Perovskites. *Journal of Solid State Chemistry*, Vol. 170, No. 2, (February 2002), pp. 368-373, ISSN: 0022-4596

Pollert, E.; Hejtmánek, J.; Jirák, Z.; Knízek, K. & Marysko, M. (2003). Influence of Co Doping on Properties of $Pr_{0.8}Na_{0.2}Mn_{(1-y)}Co_yO_3$ Perovskites. *Journal of Solid State Chemistry*, Vol. 174. No. 2, (September 2003) pp. 466-470, ISSN: 0022-4596

Pollert, E.; Hejtmánek, J.; Jirák, Z.; Knížek, K.; Maryško, M.; Doumerc, J.P.; Grenier, J.C; & Etourneau, J. (2004). Influence of the Structure on Electric and Magnetic Properties of $La_{0.8}Na_{0.2}Mn_{1-x}Co_xO_3$ Perovskites. *Journal of Solid State Chemistry*, Vol. 177, No. 12, (December 2004), pp. 4564-4568, ISSN: 0022-4596

Qi, X; Zhou, J.; Yue, Z.X.; Gui, Z.L. & Li, L.T. (2003). A Simple Way to Prepare Nanosized $LaFeO_3$ Powders at Room Temperature. *Ceramics International*, Vol. 29, No. 3, (June 2003), pp. 347-349, ISSN: 0272-8842

Rao, C.N.R. & Gopalakrishnan, J. (1997). *New Directions in Solid State Chemistry*, 2nd ed., Cambridge University Press, ISBN: 0521495598, Cambridge

Rao, C.N.R. & Raveau, B. (1998). *Colossal Magnetoresistance, Charge Ordering and Related Properties of Manganese Oxides*, World Scientific, ISBN: 9810232764, Singapure.

Rietveld, H.M. (1969). A Profile Refinement Method for Nuclear and Magnetic Structures. *Journal of Applied Crystallography*, Vol. 2, (June 1969), pp. 65-71, ISSN: 0021-8898

Rodríguez-Martínez, L.M. & Attfield, J.P. (1996). Cation Disorder and Size Effects in Magnetoresistive Manganese Oxide Perovskites. *Physical Review B - Condensed Matter and Materials Physics*, Vol. 54, No. 22, (December 1996), pp. R15622–R15625, ISSN: 0163-1829

Royer, S.; Berube, F.S. & Kaliaguine, S. (2005). Effect Of The Synthesis Conditions on the Redox And Catalytic Properties in Oxidation Reactions of $LaCo_{1-x}Fe_xO_3$, *Applied Catalysis A: General*, Vol. 282, No. 1-2, (March 2005), pp. 273-284, ISSN: 0926-860X

Safari, A.; Panda, R. K. & Janas, V. F. (1996). Ferroelectricity. Materials, Characteristics, and Applications. *Key Engineering Materials*, Vol. 122-124, (1996), pp. 35-69, ISSN: 1013-9826

Segal, D. (1989). *Chemical Synthesis of Advanced Ceramic Materials*, Cambridge University Press, ISBN: 9780521354363, Cambridge

Senna, M. (2005). A Straight Way toward Phase Pure Complex Oxides. *Journal of the European Ceramic Society,* Vol. 25, No. 12, (March 2005), pp. 1977-1984, ISSN: 0955-2219

Sfeir, J.; Vaucher, S.; Holtappels, P.; Vogt, U.; Schindler, H.-J.; Van Herle, J.; Suvorova, E.; Buffat, P.; Perret, D.; Xanthopoulos, N. & Bucheli, O. (2005). Characterization of Perovskite Powders for Cathode and Oxygen Membranes Made by Different Synthesis Routes. *Journal of the European Ceramic Society*, Vol. 25, No.12, (March 2005), pp. 1991-1995, ISSN: 0955-2219

Shannon, R.D. (1976). Revised Effective Ionic Radii and Systematic Studies of Interatomic Distances in Halides and Chalcogenides, *Acta Crystallographica*, Vol. A32, No. 5, (September 1976), pp. 751-767, ISSN: 0567-7394

Skinner, S.J. (2001). Recent Advances in Perovskite-type Materials for Solid Oxide Fuel Cell Cathodes. *International Journal of Inorganic Materials*, Vol. 3, (March 2001), pp. 113-121, ISSN: 1466-6049

Tai, L.-W; Nasrallah, M.M.; Anderson H.U.; Sparlin, D.M & Sehlin, S.R. (1995). Structure and electrical properties of $La_{1-x}Sr_xCo_{1-y}Fe_yO_3$. Part 1. The system $La_{0.8}Sr_{0.2}Co_{1-y}Fe_yO_3$, *Solid State Ionics*, Vol. 76, No. 3-4, (March 1995), pp. 259–271, ISSN: 0167-2738

Tai, M.F.; Lee, F.Y. & Shi, J.B. (2000). Co Doping Effect on the Crystal Structure, Magnetoresistance and Magnetic Properties of an $(La_{0.7}Ba_{0.3})(Mn_{1\sim x}Co_x)O_3$ System with x=0-1.0., *Journal of Magnetism and Magnetic Materials*, Vol. 209, No. 1-3, (February 2000), pp. 148-150, ISSN: 0304-8853

Takeuchi, J.; Hirahara, S.; Dhakal, T.P; Miyoshi, K. & Fujiwara, K. (2002). Cr-doping Effect on the Perovskite $(Nd,Sr)MnO_3$ Single Crystals. *Physica B: Condensed Matter*, Vol. 312-313, (March 2002), pp. 754-756, ISSN: 0921-4526

Toulemonde, O.; Studer, F.; Barnabé, A.; Maignan, A. Martin, C. & Raveau, B. (1998). Charge States of Transition Metal in "Cr, Co and Ni" Doped $Ln_{0.5}Ca_{0.5}MnO_3$ CMR Manganites. *European Physical Journal B: Condensed Matter Physics,* Vol. 4, No. 2, (April 1998) pp. 159-167, ISSN: 1434-6028

Troyanchuk, I.O.; Lobanovsky, L.S.; Khalyavin, D.D.; Pastushonok, S.N. & Szymczak, H. (2000). Magnetic and Magnetotransport properties of Co-doped Manganites with Perovskite Structure. *Journal of Magnetism and Magnetic Materials*, Vol. 210, No. 1-2, (February 2000), pp. 63-72, ISSN: 0304-8853

Ulyanov, A.N.; Kim, J.S.; Shin, G.M.; Song, K.J.; Kang, Y.M. & Yoo, S.I. (2007). $La_{0.7}Ca_{0.3}Mn_{0.95}M_{0.05}O_3$ Manganites (M ¼ Al, Ga, Fe, Mn, and In): Local Structure and Electron Configuration Effect on Curie. Temperature and Magnetization. *Physica B: Condensed Matter*, Vol. 388, No. 1-2, (January 2007), pp. 16-19, ISSN: 0921-4526

Vidal, K.; Lezama, L.; Arriortua, M.I.; Rojo, T.; Gutiérrez, J. & Barandiarán. J.M. (2005). Magnetic characterization of $Nd_{0.8}Sr_{0.2}(Mn_{1-x}Co_x)O_3$ perovskites. *Journal of Magnetism and Magnetic Materials*, Vol. 290-291, No. 2, (April 2005), pp. 914-916, ISSN: 0304-8853

Vidal, K: Rodríguez-Martínez, L.M.; Ortega-San-Martín, L.; Díez-Linaza, E.; Nó, M.L.; Rojo, T.; Laresgoiti, A. & Arriortua, M.I. (2007). Isolating the Effect of Doping in the Structure and Conductivity of $(Ln_{1-x}M_x)FeO_{3-\delta}$ Perovskites. *Solid State Ionics*, Vol. 178, No. 21-22, (July 2007), pp. 1310-1316, ISSN: 0167-2738

Vidal, K.; Rodríguez-Martínez, L.M.; Ortega-San-Martin, L.; Martínez-Amesti, A.; Nó, M.L.; Rojo, T.; Laresgoiti, A. & Arriortua, M.I. (2009). The effect of doping in the electrochemical performance of $(Ln_{1-x}M_x)FeO_{3-\delta}$ SOFC cathodes. *Journal of Power Sources*, Vol. 192, No. 1, (July 2009), pp. 175-179, ISSN: 0378-7753

Vidal, K.; Rodríguez-Martínez, L.M.; Ortega-San-Martin, L.; Nó, M.L.; Rojo, T.; Laresgoiti, A. & Arriortua, M.I. (2010). $Ln_{0.5}M_{0.5}FeO_{3-\delta}$ Perovskites as Cathode for Solid Oxide Fuel Cells: Effect of Mean Radius of the A-Site Cations. *Journal of the Electrochemical Society*, Vol. 157, No. 8, (June 2010), pp. A919-A-924, ISSN: 0013-4651

Vidal, K.; Rodríguez-Martínez, L.M.; Ortega-San-Martin, L.; Nó, M.L.; Rojo, T.; Laresgoiti, A. & Arriortua, M.I. (2011). Effect of the A Cation Size Disorder on the Properties of an Iron Perovskite Series for their Use as Cathodes for SOFCs. *Fuel Cells*, Vol. 11, No. 1, (February 2011), pp. 51-58, ISSN: 1615-6846

Wandekar, R.V.; Wani, B.N. & Bharadwaj, S.R. (2009). Crystal Structure, Electrical Conductivity, Thermal Expansion and Compatibility Studies of Co-substituted Lanthanum Strontium Manganite System. *Solid State Science*, Vol. 11, No. 1, (January 2009), pp. 240-250, ISSN: 1293-2558

Woodward, P.M.; Vogt, T.; Cox, D.E.; Arulraj, A.; Rao, C.N.R.; Karen, P. & Cheetham, A. K. (1998). Influence of Cation Size on the Structural Features of $Ln_{1/2}A_{1/2}MnO_3$ Perovskites at Room Temperature. *Chemmistry of Materials*, Vol. 10, No. 11, (October 1998), pp. 3652-3665, ISSN: 0897-4756

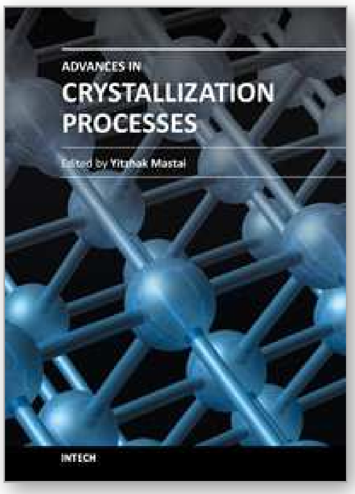

Advances in Crystallization Processes

Edited by Dr. Yitzhak Mastai

ISBN 978-953-51-0581-7
Hard cover, 648 pages
Publisher InTech
Published online 27, April, 2012
Published in print edition April, 2012

Crystallization is used at some stage in nearly all process industries as a method of production, purification or recovery of solid materials. In recent years, a number of new applications have also come to rely on crystallization processes such as the crystallization of nano and amorphous materials. The articles for this book have been contributed by the most respected researchers in this area and cover the frontier areas of research and developments in crystallization processes. Divided into five parts this book provides the latest research developments in many aspects of crystallization including: chiral crystallization, crystallization of nanomaterials and the crystallization of amorphous and glassy materials. This book is of interest to both fundamental research and also to practicing scientists and will prove invaluable to all chemical engineers and industrial chemists in the process industries as well as crystallization workers and students in industry and academia.

InTech Europe
University Campus STeP Ri
Slavka Krautzeka 83/A
51000 Rijeka, Croatia
Phone: +385 (51) 770 447
Fax: +385 (51) 686 166
www.intechopen.com

InTech China
Unit 405, Office Block, Hotel Equatorial Shanghai
No.65, Yan An Road (West), Shanghai, 200040, China
中国上海市延安西路65号上海国际贵都大饭店办公楼405单元
Phone: +86-21-62489820
Fax: +86-21-62489821